Anomalous Electrical Transport in the Kagome Magnet $YbFe_6Ge_6$

Weiliang Yao,[1,2,*] Supeng Liu,[2] Hodaka Kikuchi,[3] Hajime Ishikawa,[3] Øystein S. Fjellvåg,[4,5] David W. Tam,[4] Feng Ye,[6] Douglas L. Abernathy,[6] George D. A. Wood,[7] Devashibhai Adroja,[7,8] Chun-Ming Wu,[9] Chien-Lung Huang,[10] Bin Gao,[1] Yaofeng Xie,[1] Yuxiang Gao,[1] Karthik Rao,[1] Emilia Morosan,[1,11] Koichi Kindo,[3] Takatsugu Masuda,[3] Kenichiro Hashimoto,[2] Takasada Shibauchi,[2,†] and Pengcheng Dai[1,11,‡]

[1]*Department of Physics and Astronomy, Rice University, Houston, Texas 77005, USA*
[2]*Department of Advanced Materials Science, The University of Tokyo, Kashiwa, Chiba 277-8561, Japan*
[3]*Institute for Solid State Physics, The University of Tokyo, Kashiwa, Chiba, 277-8581, Japan*
[4]*Laboratory for Neutron Scattering and Imaging, Paul Scherrer Institut, Villigen 5232, Switzerland*
[5]*Department for Hydrogen Technology, Institute for Energy Technology, NO-2027 Kjeller, Norway*
[6]*Neutron Scattering Division, Oak Ridge National Laboratory, Oak Ridge, Tennessee 37831, USA*
[7]*ISIS Facility, STFC, Rutherford Appleton Laboratory, Chilton, Didcot, Oxfordshire OX11 0QX, United Kingdom*
[8]*Highly Correlated Matter Research Group, Physics Department, University of Johannesburg, Auckland Park 2006, South Africa*
[9]*National Synchrotron Radiation Research Center, Hsinchu 30076, Taiwan*
[10]*Department of Physics and Center for Quantum Frontiers of Research & Technology (QFort), National Cheng Kung University, Tainan 701, Taiwan*
[11]*Smalley-Curl Institute, Rice University, Houston, Texas 77005, USA*

(Received 25 June 2024; revised 1 April 2025; accepted 14 April 2025; published 6 May 2025)

Two-dimensional (2D) kagome metals offer a unique platform for exploring electron correlation phenomena derived from quantum many-body effects. Here, we report a combined study of electrical magnetotransport and neutron scattering on $YbFe_6Ge_6$, where the Fe moments in the 2D kagome layers exhibit an *A*-type collinear antiferromagnetic order below $T_N \approx 500$ K. Interactions between the Fe ions in the layers and the localized Yb magnetic ions in between reorient the *c*-axis-aligned Fe moments to the kagome plane below $T_{SR} \approx 63$ K. Our magnetotransport measurements show an intriguing anomalous Hall effect (AHE) that emerges in the spin-reorientated collinear state, accompanied by the closing of the spin anisotropy gap as revealed from inelastic neutron scattering. The gapless spin excitations and the Yb-Fe interaction are able to support a dynamic scalar spin chirality, which explains the observed AHE. Therefore, our Letter demonstrates that spin fluctuations may provide an additional scattering channel for the conduction electrons and give rise to AHE even in a collinear antiferromagnet.

DOI: 10.1103/PhysRevLett.134.186501

The Hall effect, discovered by Edwin Hall, is the potential difference across an electric conductor transverse to the current and to an externally applied magnetic field perpendicular to the current [1]. For conventional metals or semiconductors, the ordinary Hall effect (voltage) is linearly proportional to the applied magnetic field. The anomalous Hall effect (AHE), one of the most prominent phenomena of quantum transport in correlated electron materials, describes unconventional electron deflection other than the effect of external magnetic fields [2–4]. While the initial observation of AHE was made in ferromagnets (conventional AHE) [2], AHE can also occur in materials without net magnetization. The observation o f AHE in antiferromagnets is of particular interest, where the interplay of itinerant electrons and spin texture (i.e., magnetic structure) gives rise to this unique transport property [5–7]. From the application perspective, antiferromagnetic (AFM) spintronic devices have advantages over ferromagnetic counterparts, such as the absence of stray fields and being robust to external magnetic field perturbation [8].

Therefore, a determination of the microscopic origin of the AHE in antiferromagnets has been attracting great interest. For example, it is well known that a real-space Berry phase originating from a magnetic field-induced skyrmion lattice (noncoplanar spin texture) can produce an AHE termed "topological Hall effect" (THE) [9–14]. The noncoplanar spin texture of a skyrmion has a nonzero scalar spin chirality (SSC) $\chi_{ijk} = \mathbf{S}_i \cdot (\mathbf{S}_j \times \mathbf{S}_k)$, where $\mathbf{S}_i$, $\mathbf{S}_j$, and $\mathbf{S}_k$ are three localized spins at sites i, j, and k, respectively, that acts as a fictitious magnetic field to induce AHE [4]. The chiral spin texture of a magnetic skyrmion is often stabilized by the competition of Heisenberg and Dzyaloshinskii-Moriya interactions [9–11].

*Contact author: wy28@rice.edu
†Contact author: shibauchi@k.u-tokyo.ac.jp
‡Contact author: pdai@rice.edu

Going beyond the paradigm of the static spin effect, recent studies suggest that fluctuating spins can also contribute to the AHE by scattering the electrons, even in the spin-disordered state [15–18]. Arranging spins in a triangular motif is considered to be a favorable condition [18] as spin fluctuations could be significantly promoted by the geometrical frustration. The kagome lattice, a two-dimensional (2D) network of corner-sharing triangles, is an ideal platform to realize this mechanism. Indeed, spin-fluctuation-driven AHE/THE was recently observed in some kagome magnets, including AMn_6Sn_6 (A = Y, Sc, and Er) [19–22], $B_3Ru_4Al_{12}$ (B = Nd and Gd) [23,24], and HoAgGe [25]. In these materials, nonzero time-averaged SSC $\langle \mathbf{S}_i \cdot (\mathbf{S}_j \times \mathbf{S}_k) \rangle$ is induced by spin fluctuations out of noncollinear magnetic structures or paramagnetic states. However, there is no direct evidence of such spin fluctuations, for example, by inelastic neutron scattering (INS) experiments, particularly in the temperature region where the AHE was detected. In addition, it is still unclear whether spin fluctuations from collinear AFM structures can have $\langle \mathbf{S}_i \cdot (\mathbf{S}_j \times \mathbf{S}_k) \rangle \neq 0$ and therefore AHE/THE.

Here we report the discovery of a spin-fluctuation-driven AHE in the kagome lattice magnet $YbFe_6Ge_6$ with a collinear AFM structure [26–30]. Through a comprehensive study of magnetization, magnetotransport, and neutron diffraction on single crystals, we find that the AHE emerges in its spin-reorientated state below $T_{SR} \approx 63$ K, where the collinear Fe spins rotate from the c axis to the kagome plane. The combined space inversion and time-reversal ($\mathcal{IT}$) symmetry of the magnetic structure rules out the static nonzero SSC being the origin of the AHE [5–7]. Since our INS experiments reveal gapless low-energy spin excitations in the spin-reoriented state, the highly fluctuating Fe spins can contribute to a dynamic nonzero SSC by interacting with the Yb spins, which induces the AHE [31].

The crystal structure of $YbFe_6Ge_6$ is shown in Fig. 1(a), where the Fe ions form a 2D kagome lattice. $YbFe_6Ge_6$ belongs to the family of hexagonal RFe_6Ge_6 compounds (with R = Sc, Yb, Lu, Mg, Ti, Zr, Hf, and Nb) [26,28,32–34]. Their structure is derived by inserting the R ions into the B35 structure FeGe [35]. Despite the fact that they all have a Néel temperature well above room temperature, $YbFe_6Ge_6$ is the only member exhibiting a spontaneous spin reorientation (SR) transition [26,28,32–34]. Yb has been determined to be trivalent, yet its triangular lattice does not order at least above 0.4 K [27,28,36]. Thus the magnetism of $YbFe_6Ge_6$ is mainly given by the Fe kagome lattice, although there must also be Yb-Fe interactions at low temperatures.

The zero-field resistivity of $YbFe_6Ge_6$ along the kagome plane is presented in Fig. 1(b), which shows a typical metallic behavior with a residual-resistivity ratio of ~12. The derivative of the resistivity shows a small yet sharp peak around T_{SR}, indicating the change of magnetic structure. Figure 1(c) shows the DC magnetic susceptibility under a magnetic field of 1 T along and perpendicular to the

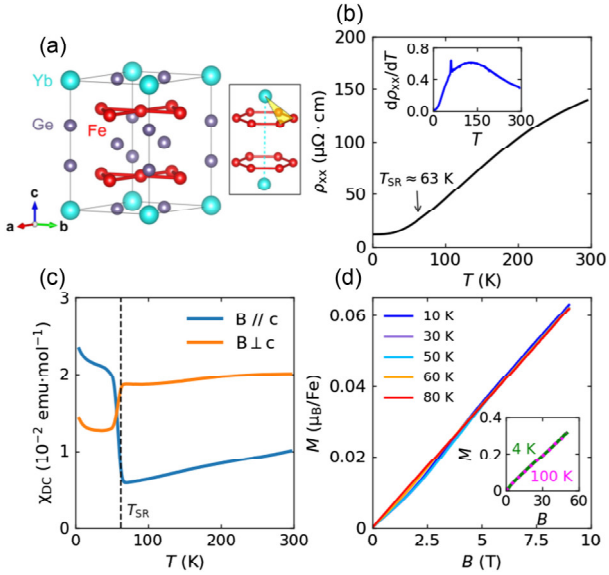

FIG. 1. (a) Crystal structure of $YbFe_6Ge_6$. Right inset shows the local structure of Yb and Fe, with one spin triad of Yb-Fe highlighted in yellow. (b) Temperature dependence of zero-field resistivity in the kagome plane. Inset shows its derivative with respect to temperature. (c) Temperature dependence of DC magnetic susceptibility under a field of 1 T parallel and perpendicular to the c axis. (d) Isothermal magnetizations along the $\mathbf{a}^*$ direction up to 9 T at selected temperatures. Inset shows the magnetizations up to 50 T at 4 K and 100 K.

c axis. The sudden susceptibility change around 63 K confirms the occurrence of the SR transition. These electrical and magnetic characteristics are consistent with an early report [28].

Next, we explore how external fields affect the magnetic and transport properties of $YbFe_6Ge_6$. Figure 1(d) presents the isothermal magnetization along the $\mathbf{a}^*$ direction at selected temperatures from 10 K to 100 K. Although the magnetization shows an overall linear dependence on the field, it is slightly nonlinear at low fields for $T < T_{SR}$. However, the magnitude of magnetization is quite small. Even at a magnetic field of 50 T, the moment size is only about 0.3 μ_B/Fe [inset of Fig. 1(d)], which is much smaller than the full moment size of ~1.5 μ_B/Fe [26,27,29,30,36]. The contrast between $T > T_{SR}$ and $T < T_{SR}$ can be more clearly discerned in the magnetoresistance (MR) [Fig. 2(a)], with $\mathrm{MR} = [\rho_{xx}(B) - \rho_{xx}(0\ \mathrm{T})]/\rho_{xx}(0\ \mathrm{T})$. Here the magnetic field is also applied along the $\mathbf{a}^*$ direction. At 80 K, the MR has an approximately quadratic dependence on the field up to 12 T. When cooling below T_{SR}, it first increases rapidly at low field and then shows the approximately quadratic behavior at high fields. Similar MR behavior was observed in Fe_3Sn_2, which is typical of metallic magnets with an SR transition [55,56].

Field dependence of the Hall resistivity is shown in Fig. 2(b), where we find a drastic change of ρ_{yx} from 10 K to 80 K. In magnetic systems, the Hall resistivity can be

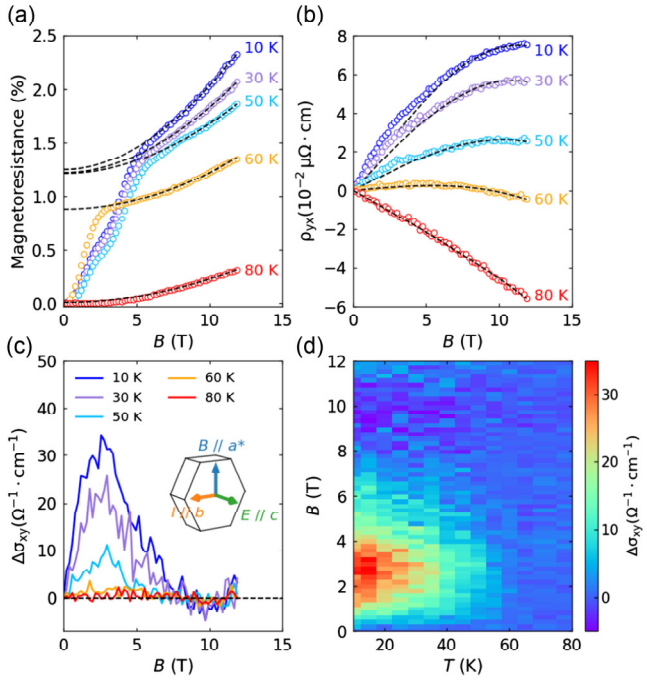

FIG. 2. (a) Magnetoresistance at selected temperatures under fields along the $\mathbf{a}^*$ direction. The electric current is along the b axis. (b) Hall resistivity at selected temperatures under fields along the $\mathbf{a}^*$ direction. Dashed curves in (a) and (b) are the fits with the two-band model [36]. (c) Remnant Hall conductivity ($\Delta\sigma_{xy}$) after subtracting the ordinary Hall contribution. Inset shows the Hall measurement configuration. (d) Contour plot of $\Delta\sigma_{xy}$ for temperatures from 10 K to 80 K and magnetic fields from 0 T to 12 T.

decomposed into three parts: $\rho_{yx} = \rho_{yx}^{\mathrm{O}} + \rho_{yx}^{\mathrm{A}} + \Delta\rho_{yx}$ [31,57], where ρ_{yx}^{O} is ordinary Hall resistivity, ρ_{yx}^{A} is conventional anomalous Hall resistivity due to net magnetization ($\rho_{yx}^{\mathrm{A}} \propto M$), and $\Delta\rho_{yx}$ is additional AHE contributions that cannot be included in the former two parts. For a magnetic system with localized moments, $\Delta\rho_{yx}$ usually comes from static and/or dynamic spin textures. In our case, M is very small and shows barely temperature dependence [Fig. 1(d)], which is in contrast to the temperature evolution of ρ_{yx} [Fig. 2(b)]. Therefore, ρ_{yx}^{A} is negligible, and we focus on the remaining two parts.

The nonlinear field dependence of MR and ρ_{yx} indicates a dominant multiband behavior. We use a two-band model to simultaneously fit the MR and ρ_{yx} [56,58,59]. Although the data at high fields can be well described by the two-band model, evident deviation from it at the low field region can be observed below T_{SR} [Figs. 2(a) and 2(b)], indicating a contribution from $\Delta\rho_{yx}$. Figure 2(c) shows the corresponding Hall conductivity $\Delta\sigma_{xy}$, where it only appears below T_{SR}. With more detailed measurements at intermediate temperatures [36], we construct a contour plot of $\Delta\sigma_{xy}$, which shows a remarkable similarity to those metallic magnets with novel Hall effects [10,57].

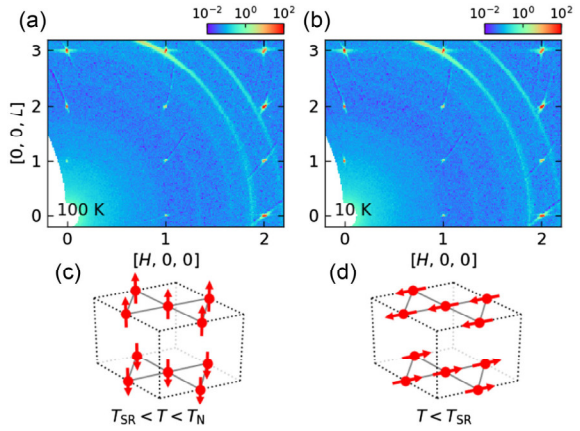

FIG. 3. (a) and (b) Neutron diffraction patterns of the $(H, 0, L)$ plane at 100 K and 10 K, respectively. The intensity color bar is in log scale to highlight possible weak features. (c) and (d) Magnetic structures of the Fe kagome lattice above and below T_{SR}, respectively.

The maximum magnitude of the Hall conductivity at 10 K is about 30 Ω^{-1} cm^{-1}, comparable with those in previous "anomalous Hall antiferromagnets" [7]. For magnetic fields applied perpendicular to the kagome plane, however, we do not observe such an AHE [36], suggesting its close connection to the magnetic anisotropy as will be discussed below.

As the anomalous electrical transport is closely related to the SR, knowing the change of the magnetic structure across T_{SR} is crucial to uncovering its origin. We hence use single crystal neutron diffraction to study the magnetic structure of $YbFe_6Ge_6$. Figure 3(a) shows the diffraction pattern of the $(H, 0, L)$ plane at 100 K ($> T_{\mathrm{SR}}$). There are no additional Bragg peaks except those at integer-index positions, consistent with the well-established A-type AFM structure with a propagation wave vector $\mathbf{k}_{\mathrm{m}} = (0, 0, 0)$ [Fig. 3(c)] [27,29,30]. When cooling down to 10 K ($< T_{\mathrm{SR}}$), the diffraction pattern is strikingly similar [Fig. 3(b)]—no additional peaks appear, while the peak intensities have clear temperature-dependent behavior due to the SR [36]. This suggests that the $\mathbf{k}_{\mathrm{m}}$ of $YbFe_6Ge_6$ remains (0, 0, 0) below T_{SR}. Representation analysis based on this propagation wave vector shows that only a collinear structure with the spins along the a axis [Fig. 3(d)] is compatible with the experiment. The SR transition in $YbFe_6Ge_6$ therefore equivalently flips the Néel vector by 90°. More details of the magnetic structure analysis can be found in [36]. The magnetic structure below T_{SR} along with the lattice space group $P6/mmm$ ensures that the system preserves $\mathcal{I}\mathcal{T}$ symmetry. With small-angle neutron scattering, we also confirmed that no field-induced peaks appear under magnetic fields along the $\mathbf{a}^*$ direction [36]. These observations rule out that the observed AHE is induced by static spin textures, such as magnetic skyrmions [13], which are restricted by Berry curvature that

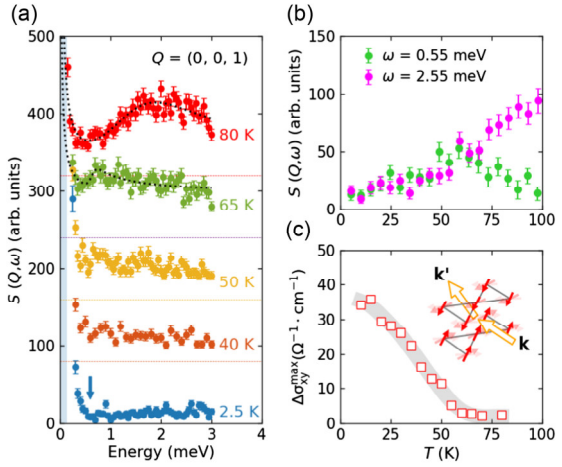

FIG. 4. (a) Low-energy spin excitations at (0, 0, 1) at selected temperatures, offset for clarity. Horizontal dashed lines indicate the zero intensity for the data above 2.5 K. Dashed curves are the fits to 65 K and 80 K data [36]. The light blue region shows energy resolution, and the arrow marks 0.6 meV, below which gapless excitations emerge. (b) Temperature dependence of the intensities at (0, 0, 1) at 0.55 meV and 2.55 meV. (c) Temperature dependence of the maximum magnitudes of $\Delta\sigma_{xy}$. The bold gray curve is a guide to the eyes. Inset illustrates electron scattering by the spin fluctuations.

requires the absence of $\mathcal{IT}$ symmetry [4,6,60]. Conversely, the spin-fluctuation-driven AHE (or THE) is not necessarily dictated by this symmetry as it originates from electron scattering by dynamic spins [15–18].

Since $YbFe_6Ge_6$ has localized magnetic moments, spin fluctuations below T_N are spin waves (magnons), which could impact the motion of conduction electrons [15]. Hence, we use INS to directly probe the magnons and determine their temperature evolution. Figure 4(a) shows the energy dependence of the INS intensities at (0, 0, 1). At 2.5 K, some INS intensities extend to ~0.6 meV, which is much larger than our instrumental energy resolution (~0.14 meV). Therefore, the spin excitations are gapless in nature. As the temperature increases, their intensity significantly increases, but they remain gapless until 50 K. When the temperature goes beyond T_{SR}, the intensity of the low-energy part starts to decrease. A broad peak centering around 2 meV shows up at 80 K, indicating the opening of a spin-wave gap. Such a gap opening behavior suggests that the magnetic anisotropy of $YbFe_6Ge_6$ transfers from an easy-plane type below T_{SR} to an easy-axis type above T_{SR}, consistent with the magnetic structures presented in Figs. 3(c) and 3(d). By fitting the data with an error function multiplied by the Bose factor [36,61], we can extract gap sizes of 0.64(4) meV and 1.34(5) meV at 65 K and 80 K, respectively.

To determine the evolution of the spin-wave gap, we show the temperature dependence of the intensities at (0, 0, 1) at 0.55 meV and 2.55 meV [Fig. 4(b)], which are located below and above the spin-wave gap, respectively. Below T_{SR}, the intensities at both energies increase as the temperature goes up. However, they start to bifurcate at T_{SR}—while the intensity above the spin-wave gap continues increasing, the intensity below it starts to decrease. The continuous increase of the intensity at 0.55 meV below T_{SR} further suggests that it is an excitation signal rather than the tail of the Bragg peak, whose intensity should otherwise decrease when the temperature approaches T_{SR}. The onset of gapless spin excitations below T_{SR} aligns with the AHE [see Fig. 4(c)], suggesting their correlation.

We point out that the gapless spin excitations below T_{SR} play a vital role in explaining the AHE through a dynamic SSC scattering mechanism, as first identified in the ferromagnetic heterostructure $SrRuO_3/SrTiO_3$ [31]. The gapless spin excitations at (0, 0, 1) within our energy resolution suggest that Fe spins can fluctuate at the cost of a very small energy, facilitating the formation of a dynamic SSC. From a semiclassical perspective, the propagation of spin waves causes adjacent Fe spins in the kagome plane to slightly deviate from the collinear ground state. On the other hand, Yb spins remain disordered above 0.4 K and thus, by themselves, have little impact on the AHE, which emerges at a much higher temperature. However, their interactions with Fe strengthen upon cooling, leading to the SR transition. Because the Yb positions and Fe kagome layers are well separated [Fig. 1(a)], the transient noncollinear Fe spin configurations and Yb spins can locally produce an SSC with $\mathbf{S}_i \cdot (\mathbf{S}_j \times \mathbf{S}_k) \neq 0$. Despite these local SSCs with opposite signs ($+$ or $-$) canceling out at zero magnetic field due to the global $\mathcal{IT}$ symmetry, a finite magnetic field partially aligns the Yb spins, resulting in a nonzero overall SSC [36]. This nonzero SSC can preferentially scatter electrons and give rise to the observed AHE. However, when the magnetic field becomes exceedingly large, low-energy spin fluctuations are suppressed due to the opening of a Zeeman gap, leading to a vanishing overall SSC and, consequently, a zero AHE. In contrast, the finite spin-wave gap above T_{SR} suggests relatively high spin stiffness. As a result, Fe spins favor maintaining the ground-state collinear configuration. Both the increased spin stiffness of the Fe kagome layer and the weaker Yb-Fe interaction at higher temperatures are unfavorable for the dynamic SSC, which accounts for the absence of the AHE above T_{SR}.

Therefore, the AHE in $YbFe_6Ge_6$ can be understood as arising from electron scattering by low-energy spin fluctuations. Given that every Fe ion has a static magnetic moment of approximately 1.5 μ_B below T_{SR} [36], we estimate a Zeeman gap of roughly 0.6 meV for a 7 T field [61,62], beyond which the AHE vanishes at low temperatures [Figs. 2(c) and 2(d)]. It suggests that the dynamic SSC contributing to the AHE is within 0.6 meV. In addition, this energy scale reasonably matches the gap size at 65 K [Fig. 4(a)], which is slightly above T_{SR}, and the AHE just disappears [Fig. 4(c)]. For comparison, we note

that the similar kagome antiferromagnet FeSn does not exhibit an AHE [63,64]. Despite also having a collinear magnetic structure with spins lying in the kagome plane, the spin waves of FeSn display a finite energy gap of ~2 meV [65,66], which suppresses low-energy spin fluctuations.

Recent experiments show that spin fluctuations can give rise to similar AHEs (or THEs) in a range of materials, including single crystals [19–25,67,68] and thin films [31,69], supporting the idea that spin-fluctuation-driven AHE is a general phenomenon. In previous studies, it depends on thermal fluctuations, with samples being heated above or close to the ordering temperature [19–25,31,67–69]. Those AHEs are therefore essentially driven by paramagnetic spin fluctuations, which are usually dominant around magnetic Bragg peak positions near the transition temperature and are gapless as well [70]. For $YbFe_6Ge_6$, the situation is different. Due to the SR transition induced by the Yb-Fe interaction, the c-axis-aligned spins transfer to the easy-plane arrangement below T_{SR}, which greatly promotes low-energy spin fluctuations even in the spin-ordered state. With the stronger Yb-Fe interaction at low temperatures, the AHE is enhanced accordingly. Moreover, $YbFe_6Ge_6$ adopts a collinear AFM structure that is much simpler than the magnetic structures of previous single crystals [19–25,67,68]. Our Letter therefore also suggests that a complex (e.g., chiral) static magnetic structure is not a prerequisite for observing spin-fluctuation-driven AHE.

In conclusion, with electrical transport, magnetization, and neutron scattering, we have systematically studied the Fe-based kagome magnet $YbFe_6Ge_6$. An AHE is observed in its AFM-ordered state when the spins are aligned parallel to the kagome plane due to the Yb-Fe interaction. The collinear magnetic structure with $\mathcal{IT}$ symmetry excludes a static SSC origin of the AHE. By directly measuring the low-energy spin excitations, we find that they become gapless at the Brillouin zone center in the spin-reoriented state. The simultaneous onset of these gapless excitations and AHE shows their close relationship and points to a dynamic SSC scattering mechanism of the latter. Our results not only reveal a spin-fluctuation-driven AHE that is not solely dependent on thermal activation but also demonstrate that dynamic spins, even in a collinear antiferromagnet, can significantly impact electrical transport.

Acknowledgments—The neutron scattering and single-crystal synthesis work at Rice was supported by U.S. NSF-DMR-2401084 and by the Robert A. Welch Foundation under Grant No. C-1839 (P. D.), respectively. The transport work at the University of Tokyo was supported by Grant-in-Aid for Scientific Research (KAKENHI) (Grant No. JP22H00105), Grant-in-Aid for Scientific Research on Innovative Areas "Quantum Liquid Crystals" (Grant No. JP19H05824) and Grant-in-Aid for Transformative Research Areas (A) "Correlation Design Science" (Grant No. JP25H01248) from Japan Society for the Promotion of Science. W. Y. acknowledges support from the US NSF-OISE-2201516 under the Accelnet program of the Office of International Science and Engineering (OISE). P. D. also acknowledges travel support from the U.S. NSF-OISE-2201516. A portion of this research used resources at the Spallation Neutron Source, a DOE Office of Science User Facility operated by the Oak Ridge National Laboratory. The beam time was allocated to CORELLI on Proposal No. IPTS-31865.1 and ARCS on Proposal No. IPTS-32630.1. The experiment at the ISIS Neutron and Muon Source was supported by a beam time allocation No. RB2410134 [71] from the Science and Technology Facilities Council. Ø. S. F. acknowledges funding from the Research Council of Norway through Project No. 325345. This work is in part based on work performed at the DMC instrument at SINQ at the Paul Scherrer Institute. Small-angle neutron scattering was performed at QUOKKA, ANSTO under Proposal No. P18792. C. L. H. acknowledges the support by the National Science and Technology Council in Taiwan (NSTC No. 113-2112-M-006-027).

[1] E. H. Hall, Am. J. Math. **2**, 287 (1879).
[2] E. H. Hall, Philos. Mag. **12**, 157 (1881).
[3] G. Bergmann, Phys. Today **32**, No. 8, 25 (1979).
[4] N. Nagaosa, J. Sinova, S. Onoda, A. H. MacDonald, and N. P. Ong, Rev. Mod. Phys. **82**, 1539 (2010).
[5] S. Nakatsuji, N. Kiyohara, and T. Higo, Nature (London) **527**, 212 (2015).
[6] H. Chen, Q. Niu, and A. H. MacDonald, Phys. Rev. Lett. **112**, 017205 (2014).
[7] L. Šmejkal, A. H. MacDonald, J. Sinova, S. Nakatsuji, and T. Jungwirth, Nat. Rev. Mater. **7**, 482 (2022).
[8] E. V. Gomonay and V. M. Loktev, Low Temp. Phys. **40**, 17 (2014).
[9] N. Kanazawa, Y. Onose, T. Arima, D. Okuyama, K. Ohoyama, S. Wakimoto, K. Kakurai, S. Ishiwata, and Y. Tokura, Phys. Rev. Lett. **106**, 156603 (2011).
[10] T. Kurumaji, T. Nakajima, M. Hirschberger, A. Kikkawa, Y. Yamasaki, H. Sagayama, H. Nakao, Y. Taguchi, T.-h. Arima, and Y. Tokura, Science **365**, 914 (2019).
[11] M. Hirschberger, T. Nakajima, S. Gao, L. Peng, A. Kikkawa, T. Kurumaji, M. Kriener, Y. Yamasaki, H. Sagayama, H. Nakao, K. Ohishi, K. Kakurai, Y. Taguchi, X. Yu, T.-h. Arima, and Y. Tokura, Nat. Commun. **10**, 5831 (2019).
[12] G. Kimbell, C. Kim, W. Wu, M. Cuoco, and J. W. A. Robinson, Commun. Mater. **3**, 19 (2022).
[13] N. Nagaosa and Y. Tokura, Nat. Nanotechnol. **8**, 899 (2013).
[14] The distinction between "anomalous Hall effect" and "topological Hall effect" in the literature is ambiguous. Sometimes, the anomalous Hall effect is broadly used to refer to the topological Hall effect, as also noted by [12]. In this Letter, since we do not discuss the topological property, we use the anomalous Hall effect to refer to the Hall effect other than the ordinary one.
[15] S. A. Yang, H. Pan, Y. Yao, and Q. Niu, Phys. Rev. B **83**, 125122 (2011).

[16] W.-T. Hou, J.-X. Yu, M. Daly, and J. Zang, Phys. Rev. B **96**, 140403(R) (2017).
[17] H. Ishizuka and N. Nagaosa, Sci. Adv. **4**, eaap9962 (2018).
[18] H. Ishizuka and N. Nagaosa, Phys. Rev. B **103**, 235148 (2021).
[19] N. J. Ghimire, R. L. Dally, L. Poudel, D. Jones, D. Michel, N. T. Magar, M. Bleuel, M. A. McGuire, J. Jiang, J. Mitchell, J. W. Lynn, and I. I. Mazin, Sci. Adv. **6**, eabe2680 (2020).
[20] Q. Wang, K. J. Neubauer, C. Duan, Q. Yin, S. Fujitsu, H. Hosono, F. Ye, R. Zhang, S. Chi, K. Krycka, H. Lei, and P. Dai, Phys. Rev. B **103**, 014416 (2021).
[21] H. Zhang, C. Liu, Y. Zhang, Z. Hou, X. Fu, X. Zhang, X. Gao, and J. Liu, Appl. Phys. Lett. **121**, 202401 (2022).
[22] K. Fruhling, A. Streeter, S. Mardanya, X. Wang, P. Baral, O. Zaharko, I. I. Mazin, S. Chowdhury, W. D. Ratcliff, and F. Tafti, Phys. Rev. Mater. **8**, 094411 (2024).
[23] K. K. Kolincio, M. Hirschberger, J. Masell, S. Gao, A. Kikkawa, Y. Taguchi, T. hisa Arima, N. Nagaosa, and Y. Tokura, Proc. Natl. Acad. Sci. U.S.A. **118**, e2023588118 (2021).
[24] K. K. Kolincio, M. Hirschberger, J. Masell, T.-h. Arima, N. Nagaosa, and Y. Tokura, Phys. Rev. Lett. **130**, 136701 (2023).
[25] S. Roychowdhury, K. Samanta, S. Singh, W. Schnelle, Y. Zhang, J. Noky, M. G. Vergniory, C. Shekhar, and C. Felser, Proc. Natl. Acad. Sci. U.S.A. **121**, e2401970121 (2024).
[26] G. Venturini, R. Welter, and B. Malaman, J. Alloys Compd. **185**, 99 (1992).
[27] T. Mazet and B. Malaman, J. Phys. Condens. Matter **12**, 1085 (2000).
[28] M. A. Avila, T. Takabatake, Y. Takahashi, S. L. Bud'ko, and P. Canfield, J. Phys. Condens. Matter **17**, 6969 (2005).
[29] J. M. Cadogan and D. H. Ryan, J. Phys. Condens. Matter **22**, 016009 (2009).
[30] D. H. Ryan, J. M. Cadogan, and R. Gagnon, J. Phys. Conf. Ser. **217**, 012124 (2010).
[31] W. Wang, M. W. Daniels, Z. Liao, Y. Zhao, J. Wang, G. Koster, G. Rijnders, C.-Z. Chang, D. Xiao, and W. Wu, Nat. Mater. **18**, 1054 (2019).
[32] T. Mazet, O. Isnard, and B. Malaman, Solid State Commun. **114**, 91 (2000).
[33] T. Mazet and B. Malaman, J. Alloys Compd. **325**, 67 (2001).
[34] T. Mazet, V. Ban, R. Sibille, S. Capelli, and B. Malaman, Solid State Commun. **159**, 79 (2013).
[35] G. Venturini, Z. Krist.-Cryst. Mater. **221**, 511 (2006).
[36] See Supplemental Material at http://link.aps.org/supplemental/10.1103/PhysRevLett.134.186501 for additional data and analyses, which includes Refs. [37–54].
[37] V. Petříček, M. Dušek, and L. Palatinus, Z. Krist.-Cryst. Mater. **229**, 345 (2014).
[38] L. Ye, T. Suzuki, and J. G. Checkelsky, Phys. Rev. B **95**, 174405 (2017).
[39] D. Ram, J. Singh, M. K. Hooda, O. Pavlosiuk, V. Kanchana, Z. Hossain, and D. Kaczorowski, Phys. Rev. B **107**, 085137 (2023).
[40] F. Ye, Y. Liu, R. Whitfield, R. Osborn, and S. Rosenkranz, J. Appl. Crystallogr. **51**, 315 (2018).
[41] A. Wills, J. Phys. IV (France) **11**, Pr9 (2001).
[42] J. Rodríguez-Carvajal, Physica (Amsterdam) **192B**, 55 (1993).
[43] G. Shirane, S. M. Shapiro, and J. M. Tranquada, *Neutron Scattering with a Triple-Axis Spectrometer: Basic Techniques* (Cambridge University Press, Cambridge, England, 2002).
[44] D. C. Johnston, Phys. Rev. Lett. **109**, 077201 (2012).
[45] D. C. Johnston, Phys. Rev. B **96**, 104405 (2017).
[46] J. Bernhard, B. Lebech, and O. Beckman, J. Phys. F **14**, 2379 (1984).
[47] A. Neubauer, C. Pfleiderer, B. Binz, A. Rosch, R. Ritz, P. G. Niklowitz, and P. Böni, Phys. Rev. Lett. **102**, 186602 (2009).
[48] Y. Tokura and N. Kanazawa, Chem. Rev. **121**, 2857 (2021).
[49] K. Wood *et al.*, J. Appl. Crystallogr. **51**, 294 (2018).
[50] D. L. Abernathy, M. B. Stone, M. J. Loguillo, M. S. Lucas, O. Delaire, X. Tang, J. Y. Y. Lin, and B. Fultz, Rev. Sci. Instrum. **83**, 015114 (2012).
[51] R. Bewley, R. Eccleston, K. McEwen, S. Hayden, M. Dove, S. Bennington, J. Treadgold, and R. Coleman, Physica (Amsterdam) **385-386B**, 1029 (2006).
[52] O. Arnold *et al.*, Nucl. Instrum. Methods Phys. Res., Sect. A **764**, 156 (2014).
[53] R. Ewings, A. Buts, M. Le, J. van Duijn, I. Bustinduy, and T. Perring, Nucl. Instrum. Methods Phys. Res., Sect. A **834**, 132 (2016).
[54] H. Kikuchi, S. Asai, T. J. Sato, T. Nakajima, L. Harriger, I. Zaliznyak, and T. Masuda, J. Phys. Soc. Jpn. **93**, 091004 (2024).
[55] N. Kumar, Y. Soh, Y. Wang, and Y. Xiong, Phys. Rev. B **100**, 214420 (2019).
[56] L. Wang, J. Zhu, H. Chen, H. Wang, J. Liu, Y.-X. Huang, B. Jiang, J. Zhao, H. Shi, G. Tian, H. Wang, Y. Yao, D. Yu, Z. Wang, C. Xiao, S. A. Yang, and X. Wu, Phys. Rev. Lett. **132**, 106601 (2024).
[57] T. Suzuki, R. Chisnell, A. Devarakonda, Y.-T. Liu, W. Feng, D. Xiao, J. W. Lynn, and J. Checkelsky, Nat. Phys. **12**, 1119 (2016).
[58] N. W. Ashcroft and N. D. Mermin, *Solid State Physics* (Holt-Saunders, New York, 1976).
[59] Z. Zhu, B. Fauqué, K. Behnia, and Y. Fuseya, J. Phys. Condens. Matter **30**, 313001 (2018).
[60] X.-Y. Hou, H.-C. Yang, Z.-X. Liu, P.-J. Guo, and Z.-Y. Lu, Phys. Rev. B **107**, L161109 (2023).
[61] L. Chen, X. Teng, H. Tan, B. L. Winn, G. E. Granorth, F. Ye, D. H. Yu, R. A. Mole, B. Gao, B. Yan, M. Yi, and P. Dai, Nat. Commun. **15**, 1918 (2024).
[62] X. Teng *et al.*, Nature (London) **609**, 490 (2022).
[63] B. C. Sales, J. Yan, W. R. Meier, A. D. Christianson, S. Okamoto, and M. A. McGuire, Phys. Rev. Mater. **3**, 114203 (2019).
[64] M. Kang *et al.*, Nat. Mater. **19**, 163 (2020).
[65] Y. Xie, L. Chen, T. Chen, Q. Wang, Q. Yin, J. R. Stewart, M. B. Stone, L. L. Daemen, E. Feng, H. Cao, H. Lei, Z. Yin, A. H. MacDonald, and P. Dai, Commun. Phys. **4**, 240 (2021).
[66] S.-H. Do, K. Kaneko, R. Kajimoto, K. Kamazawa, M. B. Stone, J. Y. Y. Lin, S. Itoh, T. Masuda, G. D. Samolyuk, E. Dagotto, W. R. Meier, B. C. Sales, H. Miao, and A. D. Christianson, Phys. Rev. B **105**, L180403 (2022).
[67] N. Abe, Y. Hano, H. Ishizuka, Y. Kozuka, T. Tadano, Y. Tsujimoto, K. Yamaura, S. Ishiwata, and J. Fujioka, npj Quantum Mater. **9**, 41 (2024).
[68] H. Jeon, H. Seo, J. Seo, Y. H. Kim, E. S. Choi, Y. Jo, H. N. Lee, J. M. Ok, and J. S. Kim, Commun. Phys. **7**, 162 (2024).

[69] Y. Fujishiro, N. Kanazawa, R. Kurihara, H. Ishizuka, T. Hori, F. S. Yasin, X. Yu, A. Tsukazaki, M. Ichikawa, M. Kawasaki, N. Nagaosa, M. Tokunaga, and Y. Tokura, Nat. Commun. **12**, 317 (2021).
[70] M. F. Collins and W. Marshall, Proc. Phys. Soc. **92**, 390 (1967).
[71] W. Yao, G. Wood, P. Dai, B. Gao, and D. Adroja, Spin wave and crystal field excitations in a Fe-based Kagome magnet, STFC ISIS Neutron and Muon Source (2024), 10.5286/ISIS.E/ISIS.E.RB2410134.

End Matter

Appendix—While dispersive spin waves of $YbFe_6Ge_6$ extend to much higher energies, only the low-energy part (i.e., the spin-wave gap) shows a significant change across T_{SR}. Figures 5(a) and 5(b) show the excitation spectra along the $[0, 0, L]$ direction at 10 K and 100 K, respectively [36]. The signals around $L = 1$ and 3 are magnons, while phonons appear at larger momentum transfer positions. The overall excitation spectrum changes little except for the intensity, as can be seen from the constant-energy cuts shown in Figs. 5(c) and 5(d). We notice that the intensity increase from 10 K to 100 K is significantly larger than the effect simply due to the Bose factor [gray curves in Figs. 5(c) and 5(d)], indicating a change of spin orientation. Thermal evolution of the low-energy spin excitations around (0, 0, 1) is presented in Figs. 5(e)–5(i) [36]. Since the magnon has a bandwidth of ~40 meV along the [0, 0, L] direction [36], the spin excitations below 3 meV are rodlike and concentrated at the Brillouin zone center. As the temperature rises to near T_{SR}, their intensity gradually accumulates, which extends down to the elastic background [Figs. 5(e)–5(h)]. However, the intensity around 1 meV drops at 80 K ($> T_{SR}$) [Fig. 5(i)], indicating the presence of an energy gap, consistent with the data shown in Fig. 4.

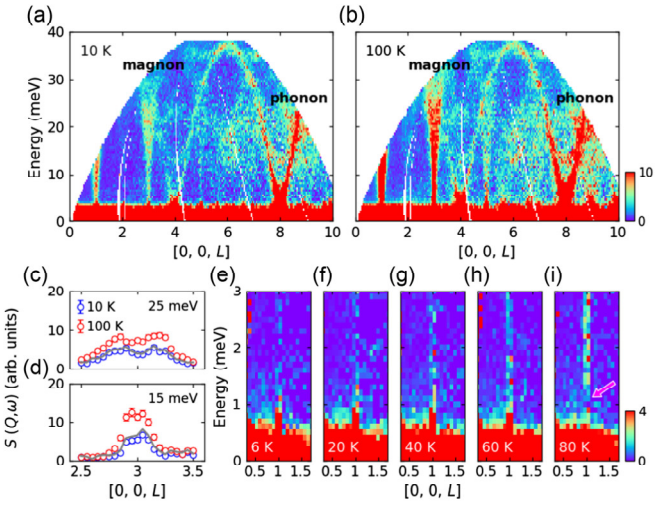

FIG. 5. (a) and (b) Excitation spectra along the $[0, 0, L]$ direction at 10 K and 100 K, respectively. (c) and (d) Constant energy cuts around (0, 0, 3) at 25 meV and 15 meV, respectively. Gray curves represent the calculated intensities at 100 K by correcting the 10 K data with the Bose factor. (e)–(i) Low-energy spin excitations around (0, 0, 1) at selected temperatures. Magenta arrow indicates the energy gap at 80 K.